Characterization of alkali-activated slag paste containing dredged marine sediment

Jae-Ho Shim, Joo-Young Jeong, Jin-Young Park, Jin-Suk Ryu, Joo-Yang Park*

Department of Civil and Environmental Engineering, Hanyang University, 222 Wangsimni-ro, Seoungdong-gu, Seoul, Korea, Tel. +82 2 2296 7536; emails: jaehoshim@hanyang.ac.kr (J.-H. Shim), jooyjeong@hanyang.ac.kr (J.-Y. Jeong), pjy0678@hanyang.ac.kr (J.-Y. Park), rainer90@hanyang.ac.kr (J.-S. Ryu), jooypark@hanyang.ac.kr (J.-Y. Park)

ABSTRACT

We characterized alkali-activated slag paste containing dredged marine sediment according to Na_2O concentration by mass of slag in the mixture. The compressive strengths of 3-d cured AAS–sediment paste specimens were similar to those of 28-d cured AAS–sediment paste specimens. The optimum Na_2O concentration by mass of slag was 6–8%. Leaching testing of samples cured for 3 d confirmed that heavy metals (Cr, Cu, Cd, and Pb) were below the detection limits for all these metals. X-ray diffraction, scanning electron microscopy, and Fourier transform infrared spectroscopy analyses revealed that the microstructure, fracture surface, and silicate band of calcium silicate hydrate as the main hydrate of the AAS–sediment paste were similar among the various samples. Despite this, Ca/Si molar ratios and quantitative analysis results differed among samples with different Na_2O concentrations by mass of slag.

Keywords: Alkali activation; Dredged marine sediment; Ground-granulated blast-furnace slag (GGBFS); Solidification/stabilization (S/S)

1. Introduction

The Convention on the Prevention of Marine Pollution by Dumping of Wastes and Other Matter 1972 encourages the recycling of dredged sediment [1,2]. Recycling of smaller fine sediments (<75 μm) is difficult and uneconomical due to their small particle size, and also because fine sediments usually contain high concentrations of heavy metals [3–6]. The high concentrations of heavy metals in fine sediments are associated with the large surface areas of the smaller particles given that heavy metals tend to accumulate on particles by means of sorption and co-precipitation on the surface. Furthermore, carbonates and chlorides present in dredged marine sediments make it more difficult to treat contaminants in sediment by means of normal soil remediation techniques [2,7].

General technologies for treating contaminated dredged sediment include solidification/stabilization (S/S) [8], soil washing [9], electrokinetic remediation [2], thermal treatment [10], and vitrification [11]. S/S technology stabilizes the contaminants and reduces their mobility. S/S based on the use of cement has

*Corresponding author.

been widely used to treat metal-contaminated soil, but to use dredged fine sediment as recycling material while meeting environmental and human health requirements, the development of novel binders and processes is required. In recent years, many researchers have studied the remediation of sediment using alkali-activated binders such as slag and fly ash [12–17]. Slag and fly ash are cost-effective alkali-activated binders that can be activated by alkaline activators such as alkalis, silicates, aluminates, non-silicate weak acid salts, and aluminosilicates [18]. These alkaline activators react with Ca^{2+} from ground-granulated blast-furnace slag (GGBFS) to form less soluble compounds [19,20]. In particular, the use of GGBFS is beneficial in developing hardening materials with low concentrations of alkaline activator [21–26]. Sodium hydroxide (NaOH) solution is the most commonly used alkaline activator and is also one of the most cost effective. The main reaction product of alkali-activated slag is a calcium silicate hydrate (C–S–H) similar to that formed by Portland cement hydration [27–29]. The microstructure and properties of alkali-activated binders depend on the chemical compositions of the raw materials used, the concentration and type of alkaline activator, and curing conditions such as temperature and time [30]. In particular, the concentration of the activator can have a large influence on the mechanical properties and durability of the hardening paste. C–S–H formed as a reaction product of the slag with the alkaline activator contributes significantly to the overall strength of the resulting material [27,31–37].

Previous studies have generally focused on evaluating the effectiveness of S/S, mainly from mechanical and environmental viewpoints. It is important to determine the potential change in the compressive strength and microstructure of specimens with solidified/stabilized sediment due to the addition of an alkaline activator. Our main objectives in this study were therefore (1) to evaluate the compressive strength, (2) evaluate the effectiveness of heavy metal immobilization, and (3) investigate hardening mechanisms in the microstructure of the hydrate in alkali-activated slag containing dredged marine sediment.

2. Materials and methods

2.1. Materials

Dredged marine sediment used in this study was sampled from Nam Harbor in Busan, Korea. Sediment in the size range of 10–30 μm was collected in a plastic bag, which was then hermetically sealed to prevent any oxidation of reduced compounds. Wet sediment

was used for granulometric analysis, and dried sediment was used for all other analyses. Particle size of the sediment was characterized according to ASTM D2487. The water content, absolute density, and particle size classification are shown in Table 1. Following the maritime environment pollutant testing method in Korea, the contents of heavy metals in the sediment were analyzed. Table 2 shows the total heavy metal concentrations (average) in the dredged marine sediment.

Table 3 shows the properties of the GGBFS used as the primary binder in the present study; the GGBFS complied with the Korean Standard KS F 2563, class 3. GGBFS was analyzed by X-ray fluorescence (XRF), and its oxide content is listed in Table 4. The basicity coefficient $Kb = (CaO + MgO)/(SiO_2 + Al_2O_3)$ was 1.08. NaOH solution was used as an alkaline activator in this study; it was prepared by dissolving NaOH beads (>93% pure) in distilled water. The concentrations of alkaline activators prepared were 2, 4, 6, and 8% Na_2O by mass of slag.

2.2. Preparation of AAS paste

To keep the microstructural properties and compressive strengths of the samples constant, the collected dredged sediment was dried at 105°C. The dried sediment was premixed with GGBFS at a 1:9 ratio using a Hobart mixer. The water-to-binder ratio (binder: primary binder + anhydrous activator) was set to 0.3 in consideration of the saturated-surface-dry of the sediment. Each alkali-activated GGBFS–sediment (AAS–sediment) paste was cast into three prism molds (40 mm × 40 mm × 160 mm) on a vibrating table. All mixtures were sealed in plastic bags and then cured at 80°C for 24 h. Specimens were stored in the laboratory, where the temperature was maintained at 20 ± 1°C. Specimens were prepared in triplicate at 3, 7, and 28 d.

Table 1
Physical properties of the sediment

Parameter		Value
Water content (wt.%)		41
Absolute density (g/cm^3)		2.74
Particle size classification (wt.%)	Gravel	0.48
	Sand	95.07
	Silt	4.46
	Clay	0

Table 2
Contents of heavy metals in the dredged sediment

Cr (mg/L)	1,043
Cu (mg/L)	1,206.7
Cd (mg/L)	1.6
Pb (mg/L)	232

Table 3
GGBFS specifications

Property	Value
Density (g/cm^2)	2.90
Fineness (cm^2/g)	4,150
Flow rate (%)	99
Strength activity index—age of 7 d (%)	64
Strength activity index—age of 28 d (%)	102
Strength activity index—age of 91 d (%)	113
MgO (wt.%)	3.1
SO$_3$ (wt.%)	0.6
Loss on ignition (wt.%)	0.2
Cl$^-$ (wt.%)	0.004

Table 4
Chemical composition of GGBFS

Compound	wt.%
CaO	46.2
SiO$_2$	32.3
Al$_2$O$_3$	13.5
MgO	3.2
SO$_3$	2.0
TiO$_2$	1.0
Fe$_2$O$_3$	0.4
Other	1.4

2.3. Physical, chemical, and microstructural analytical methods

Specimens were tested to determine their flexural and compressive strengths by means of ASTM C348 and 349. After mechanical testing, broken specimens were crushed for chemical and microstructural analyses. TCLP tests using ICP-OES were performed according to TCLP method 1311 to examine the leaching characteristics of heavy metals (Cd, Cr, Cu, and Pb) in specimens cured for 3 d.

Microstructural analysis was conducted to investigate the effect of Na$_2$O concentration by mass of slag on hydrate transitions. Field-emission scanning electron microscopy combined with energy dispersive spectroscopy (FE-SEM/EDS, Carl Zeiss, SUPRA 55VP) was performed using a platinum powder coating applied by a sputter coater (BAL-TEC/SCD 005). Powder X-ray diffractometry (PXRD, Bruker, D8 Advance) and Fourier transform infrared spectroscopy (FTIR, Thermo Scientific, Nicolet 6700) were also performed. FE-SEM/EDS plots were obtained over specified regions. PXRD data over the 2θ range from 5° to 70° were collected at a constant scanning rate of 2°/min under Cu Kα radiation ($\lambda = 1.5406$ nm). FTIR absorption spectra of samples dispersed in KBr were recorded in the range of 4,000–400 cm^{-1} by scanning 32 times at a resolution of 4 cm^{-1}. Microstructural analyses were conducted using the samples cured for 3 d.

3. Results and discussion

3.1. Compressive strength development

The compressive strengths of the samples were compared to evaluate the effect of Na$_2$O concentration by mass of slag. The concentration of NaOH solution as an alkaline activator was varied to obtain a wide range of concentrations of Na$_2$O by mass of slag in the mixture. The compressive strength of the AAS–sediment paste increased with curing time and concentration of activator (Fig. 1). Compressive strength developed quite rapidly because of the initial curing for 24 h at the elevated temperature of 80°C [38–40]. The minimum difference in compressive strengths between the samples cured for 3 and 28 d was only 1.5 MPa. The compressive strength values of the 2, 4,
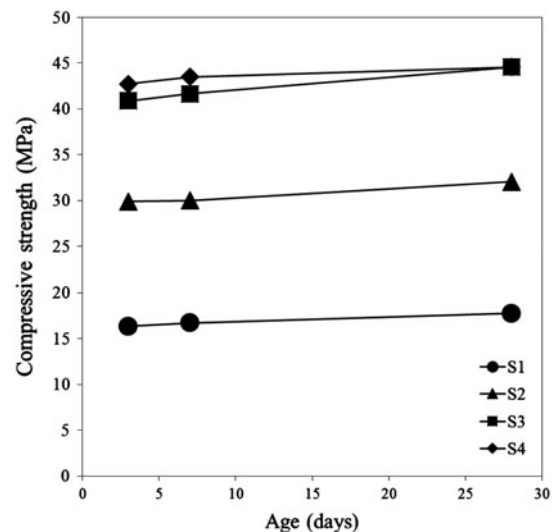
Fig. 1. Compressive strengths of AAS–sediment pastes at 3, 7, and 28 d according to the concentration of Na$_2$O relative to slag mass (S1: 2% Na$_2$O; S2: 4% Na$_2$O; S3: 6% Na$_2$O; S4: 8% Na$_2$O).

6, and 8% Na_2O–AAS–sediment pastes at 28 d were 17.8, 32.1, 44.6, and 44.6 MPa, respectively. Basically, increasing the concentration of the alkaline activator increased the strength of the specimens. However, compressive strength was not directly proportional to Na_2O concentration by mass of slag. For example, although the compressive strength of the 8% Na_2O–AAS–sediment paste was the highest among the samples prepared, its compressive strength development was similar to that of the 6% Na_2O–AAS–sediment paste. In particular, after 28 d of curing, the compressive strengths of the 6 and 8% Na_2O–AAS–sediment pastes were the same (44.6 MPa). These results suggest that the optimum Na_2O concentration by mass of slag in terms of producing the highest compressive strength is between 6 and 8%.

3.2. TCLP

All AAS–sediment paste samples cured for 3 d were subjected to TCLP testing to evaluate the effect of the S/S in immobilizing various types of heavy metals. All analyzed heavy metals (Cr, Cu, Cd, and Pb) in the TCLP leachates were below the detection limits: 0.007 mg/L for Cr, 0.006 mg/L for Cu, 0.004 mg/L for Cd, and 0.04 mg/L for Pb. We attributed the effective immobilization of leachable metals in the contaminated sediment for the 3-d cured AAS–sediment paste to rapid hardening by the initial high temperature curing [38–40]. NaOH–slag paste has a high neutralization potential and can prevent leaching and dissolution of heavy metals in a matrix of hydrates [41,42]. Because the concentrations of Cr, Cu, Cd, and Pb in the TCLP leachates from the AAS–sediment paste were below the regulated levels suggested by the United States Environmental Protection Agency, the AAS–sediment paste can be classified as a non-hazardous material. Thus, the AAS–sediment paste described in this study can be considered safe for use in various fields.

3.3. XRD analysis

XRD patterns for the AAS–sediment pastes are shown in Fig. 2. The main hydration product was C–S–H with a low degree of crystallinity as a broad feature centered at a 2θ of 29° [27,31–34]. The observed increase in intensity of XRD according to the Na_2O content in the specimens could be explained as the increase in volume or crystallinity of hydrate in the alkali-activated slag. XRD patterns of katoite, zeolite A, hydrotalcite, and quartz were also observed in the AAS–sediment pastes. Quartz is a major mineral constituent of sediment [43].

C–S–H as the main hydrate is known to be the main determinant of strength development in GGBFS [27,31–37,44–49]. However, despite the increase in compressive strength with increasing Na_2O concentration in the AAS–sediment paste, the intensities of C–S–H in the hydrates were similar. In contrast, the intensities of the XRD patterns of katoite, and zeolite A increased with increasing Na_2O concentration. Katoite is a calcium aluminum silicate hydrate (C–A–S–H) phase formed by incorporation of aluminum in C–S–H. It is also a member of the calcium aluminum garnet series in the hydrogarnet family that has more hydroxide than other calcium aluminum garnets. The hydrogarnet family $Ca_3Al_2(SiO_4)_{3-x}(OH)_{4x}$ is capable of incorporating OH^- by substitution of silicates [50–52], and hydrogarnet is classified as katoite for $1.5 < x < 3$ [53,54]. The amount of katoite in a hydrogarnet family depends on the amount of OH^- present in the activation environment. The tendency of the peak intensity of katoite to increase according to the percent of Na_2O by mass of slag was similar to the observed increase in compressive strength. This suggests that compressive strength development is correlated with the peak intensity of C–S–H and C–A–S–H. Zeolite A is usually formed in low-calcium alkali-activated binder systems. Although zeolite A is thought to be formed by reaction of high-sodium, silicate, and aluminum after formation of C–S–H, additional studies are required to confirm this. Hydrotalcite was observed in other studies of hydrates in the AAS system [27,31,32,55–57]. Hydrotalcite, as a layered double hydroxide structure, can consist of OH^-, Cl^-, or CO_3^{2-} as balancing anions. Hydrotalcite was observed at 2θ of 11.5° (Fig. 2), and hydrotalcite likely incorporated Cl^- or CO_3^{2-} in the interlayers.

3.4. FE-SEM/EDS analysis

Fracture surfaces of the AAS–sediment pastes were analyzed by FE-SEM. The fracture surfaces of samples showed relatively compact matrices of hydration products (Fig. 3). The main hydrates were C–S–H phases, described as "relatively nondescript" or consisting of "equant grains", approximately, corresponding to the Type III classification of Diamond (1976) [46]. There were no substantial differences in fracture surfaces of the AAS–sediment pastes among samples with different concentrations of Na_2O by mass of slag. This implied that C–S–H phases comprised the main hydrates in the formulations containing 2–8% Na_2O by mass of slag.

Z	Zeolite A	# 78-2453
Ht	Hydrotalcite	# 41-1428
K	Katoite	# 38-0368
Q	Quartz	# 87-2096
C(I)	C-S-H	# 34-0002
C	C-S-H	# 33-0306
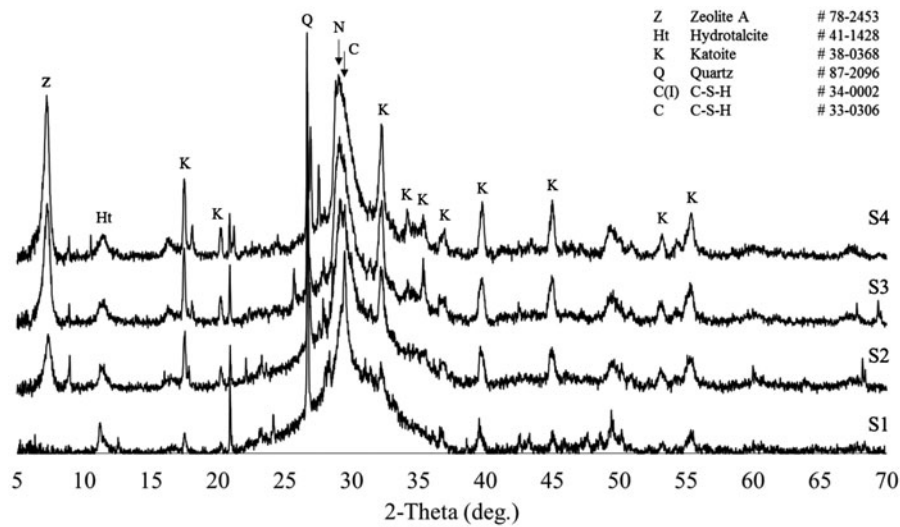
Fig. 2. XRD patterns of AAS–sediment pastes cured for 3 d (S1: 2% Na_2O; S2: 4% Na_2O; S3: 6% Na_2O; S4: 8% Na_2O).
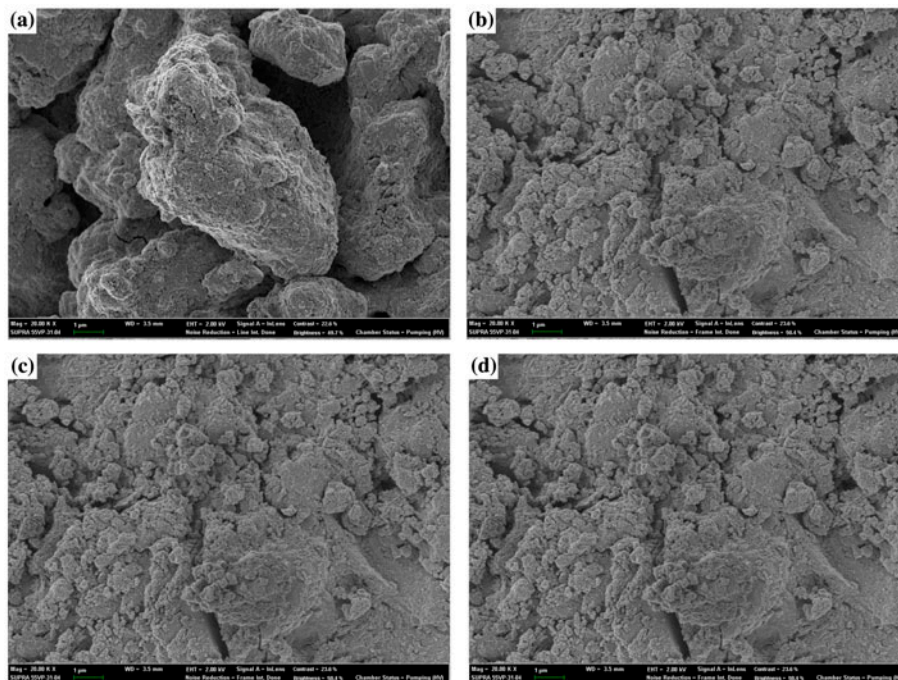
Fig. 3. SEM images of AAS–sediment pastes containing various Na_2O concentrations by mass of slag, each cured for 28 d: (a) 2% Na_2O, (b) 4% Na_2O, (c) 6% Na_2O, (d) 8% Na_2O.

To determine the chemical compositions present in the microstructures of AAS–sediment paste samples, we performed EDS analysis of the hydrates. The majority of the phases contained various elements in the bulk region, suggesting the formation of alkali-activated hydrate by polymerization throughout the interparticle volume. Microanalysis was performed using chosen points on the surface of the hydrates for each sample. Fig. 4 shows correlations between compressive strength and the Ca/Si molar ratio of the main hydrates for various concentrations of Na_2O. The Ca/Si molar ratio ranged from 2.1 to 1.53. The most favorable Ca/Si molar ratio for the development of C–S–H was between 0.66 and 2 [58]. Ca/Si molar
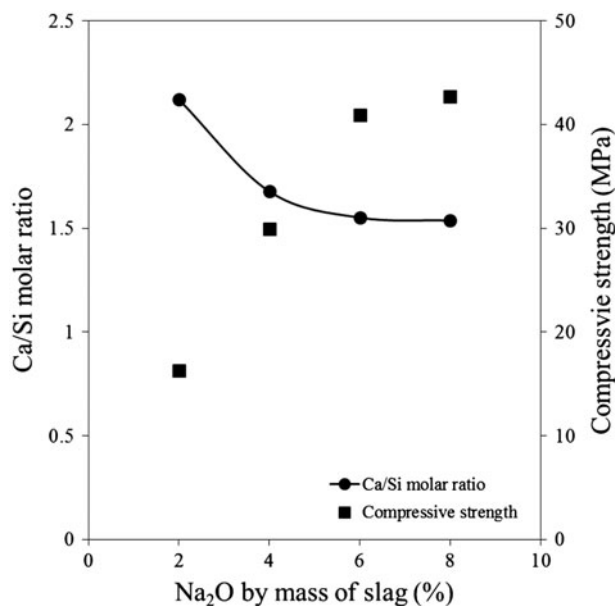
Fig. 4. Correlations between compressive strength and atomic molar ratios of the main hydrates according to Na$_2$O concentration.

3.5. FTIR spectroscopy

Spectra of the four paste samples showed analogous absorption bands (Fig. 5). All had bands at around 3,450 and 1,645 cm^{-1}, respectively, related to –OH stretching vibration and bending vibration of H:OH groups in the hydrated products [62–65]. The band near 950 cm^{-1} was attributed to the asymmetric stretching vibration mode of Si–O–T bonds (T: tetrahedral Si or Al). This band actually represents a superposition of stretching modes from both crystalline and vitreous phases. The next main band at 485 cm^{-1} was assigned to the Si–O bending mode.

All samples contained carbonate species, as indicated by the large absorption band observed around 1,450 cm^{-1} and the small one observed at 720 cm^{-1}, related to antisymmetric stretching (v_3) and out-of-plane bending (v_2) modes of CO$_3^{2-}$ ions, respectively [62,66–71].

The four paste samples had similar overall IR spectral characteristics, with the same number of apparent silicate bands and band positions. However, some dissimilarities were noted among the samples. Fundamental structural differences between the four samples were observed around 1,000–400 cm^{-1}. The full width at half maximum (FWHM) of these bands decreased as the Na$_2$O concentration by mass of slag increased. It is known that phases of non-ordered structures cause increases in bandwidths due to the existence of significant fluctuations in geometric parameters [72]. These results suggest that non-ordered phases decreased with increasing Na$_2$O concentration by mass of slag. These results were confirmed by the increase in relative diffraction peak

ratios between 2.1 and 1.53 have been classified as C–S–H(II) or γ–C–S–H in previous studies [59,60]. The Ca/Si molar ratio decreased with an increase in the percent of Na$_2$O by mass of slag, and was inversely proportional to the compressive strength. The highest compressive strength was observed at a Ca/Si molar ratio of around 1.5. A low Ca/Si molar ratio in C–S–H indicates a greater degree of polymerization, which improves the compactness of C–S–H [47,61].

Fig. 5. FTIR spectra of AAS–sediment pastes cured for 3 d (S1: 2% Na$_2$O; S2: 4% Na$_2$O; S3: 6% Na$_2$O; S4: 8% Na$_2$O).

intensity of XRD patterns with increasing Na_2O concentration by mass of slag. We attributed this to increased crystallinity in the samples, consistent with lower Ca/Si molar ratios with increasing Na_2O concentration by mass of slag [61]. The principal band associated with the Al–O and Si–O stretching vibrations near 1,000 cm^{-1} [73] is indicative of a wide distribution of SiQ^n(mAl) units in the examined structures. The Si–O stretching modes for the SiQ^n units yielded infrared absorption bands localized around 1,200, 1,100, 950, 900, and 850 cm^{-1} for $n = 4, 3, 2, 1,$ and 0, respectively [74], indicating a structure of SiQ^2(1Al) for all samples. A shoulder at about 1,030 cm^{-1} was assigned to the tetrahedral Al–O–Si asymmetric stretching vibration in aluminosilicates. The Al–O–Si vibrational bands were broad because of the amorphous structure of the aluminosilicate within the slag. The peak corresponding to Si–OH bonds, with a shoulder at 895 cm^{-1} and lower than the wavenumber of 950 cm^{-1}, became clearer as the Na_2O concentration in the paste increased. Silicon interacts with infrared radiation, and high silicon content resulted in a sharp peak at 895 cm^{-1} corresponding to Si–O stretching and OH banding. Both of these results indicated increased incorporation of Si into the C–S–H structure with increasing Na_2O concentration in the paste.

4. Conclusions

Contaminated dredged marine sediment with a fine grain size was solidified/stabilized with GGBFS using various concentrations of NaOH solution as an alkaline activator. The resulting AAS–sediment pastes showed high-compressive strength development despite containing dredged marine sediment, and heavy metal (Cr, Cu, Cd, and Pb) concentrations were all below the limits of detection in TCLP tests. Compressive strength increased with increasing Na_2O concentration by mass of slag, but this increasing tendency plateaued, with concentrations of 6 and 8% yielding the highest compressive values observed. The peak intensity of the C–A–S–H phase in the XRD peak pattern increased with increasing Na_2O concentration by mass of slag, but the extent of the increase was not directly proportional to the Na_2O concentration by mass of slag. We attributed this non-proportional relationship to diminution in the increase in peak intensity of C–A–S–H. FE-SEM images of fracture surfaces of all samples revealed compact structures of equant grains as C–S–H phases. The Ca/Si molar ratio of the C–S–H phases as determined by EDS analysis was strongly correlated with compressive strength; the highest compressive strength value was observed for a Ca/Si molar ratio of 1.5. The structure of AAS–sediment paste was confirmed to be SiQ^2(1Al) by means of FTIR and FE-SEM/EDS analyses, and there was some incorporation of Si in the C–S–H structure depending on the Na_2O concentration by mass of slag. In conclusion, when the formulation of the binder and the concentration of activator are optimized, contaminated dredged marine sediment of fine grain size can be recycled for reuse in various fields.

References

[1] S.Y. Park, G.Y. Park, D.H. Kim, J.S. Yang, K. Baek, Electrokinetic separation of heavy metals from wastewater treatment sludge, Sep. Sci. Technol. 45 (2010) 1982–1987.

[2] K.J. Kim, D.H. Kim, J.C. Yoo, K. Baek, Electrokinetic extraction of heavy metals from dredged marine sediment, Sep. Purif. Technol. 79 (2011) 164–169.

[3] F. Ackermann, A procedure for correcting the grain-size effect in heavy-metal analyses of estuarine and coastal sediments, Environ. Technol. Lett. 1 (1980) 518–527.

[4] W. Salomons, U. Förstner, Metals in the Hydrocycle, Springer-Verlag, Berlin; New York, NY, 1984.

[5] D. Martinčić, Z. Kwokal, M. Branica, Distribution of zinc, lead, cadmium and copper between different size fractions of sediments I. The Limski Kanal (North Adriatic Sea), Sci. Total Environ. 95 (1990) 201–215.

[6] G. Biksham, V. Subramanian, A.L. Ramanathan, R. Grieken, Heavy metal distribution in the Godavari River basin, Environ. Geol. Water Sci. 17 (1991) 117–126.

[7] J.F. Peng, Y.H. Song, P. Yuan, X.Y. Cui, G.L. Qiu, The remediation of heavy metals contaminated sediment, J. Hazard. Mater. 161 (2009) 633–640.

[8] C.N. Mulligan, R.N. Yong, B.F. Gibbs, An evaluation of technologies for the heavy metal remediation of dredged sediments, J. Hazard. Mater. 85 (2001) 145–163.

[9] L. Di Palma, R. Mecozzi, Heavy metals mobilization from harbour sediments using EDTA and citric acid as chelating agents, J. Hazard. Mater. 147 (2007) 768–775.

[10] C. Huang, J.R. Pan, K.D. Sun, C.T. Liaw, Reuse of water treatment plant sludge and dam sediment in brick-making, Water Sci. Technol. 44 (2001) 273–277.

[11] L.K. Wang, Y.T. Hung, H.H. Lo, C. Yapijakis, Handbook of Industrial and Hazardous Wastes Treatment, CRC Press, New York, NY, 2004.

[12] Y.L. Wei, C.Y. Lin, S.H. Cheng, H.P. Wang, Recycling steel-manufacturing slag and harbor sediment into construction materials, J. Hazard. Mater. 265 (2014) 253–260.

[13] S. Asaoka, T. Yamamoto, Blast furnace slag can effectively remediate coastal marine sediments affected by organic enrichment, Mar. Pollut. Bull. 60 (2010) 573–578.

[14] N. Vdović, G. Billon, C. Gabelle, J.L. Potdevin, Remobilization of metals from slag and polluted sediments (Case Study: The canal of the Deûle River, northern France), Environ. Pollut. 141 (2006) 359–369.

[15] D. Wang, N.E. Abriak, R. Zentar, Strength and deformation properties of Dunkirk marine sediments solidified with cement, lime and fly ash, Eng. Geol. 166 (2013) 90–99.

[16] R. Zentar, D.X. Wang, N.E. Abriak, M. Benzerzour, W.Z. Chen, Utilization of siliceous-aluminous fly ash and cement for solidification of marine sediments, Constr. Build. Mater. 35 (2012) 856–863.

[17] D.D. Tomasevic, M.B. Dalmacija, M.D. Prica, B.D. Dalmacija, D.V. Kerkez, M.R. Bečelić-Tomin, S.D. Roncevic, Use of fly ash for remediation of metals polluted sediment—Green remediation, Chemosphere 92 (2013) 1490–1497.

[18] V.D. Glukhovsky, Slag-alkali concretes produced from fine-grained aggregate, Vishcha Shkolay, Kiev, 1981.

[19] C.J. Shi, R.L. Day, Pozzolanic reaction in the presence of chemical activators, Cem. Concr. Res. 30 (2000) 607–613.

[20] C.J. Shi, R.L. Day, Some factors affecting early hydration of alkali-slag cements, Cem. Concr. Res. 26 (1996) 439–447.

[21] T.W. Cheng, J.P. Chiu, Fire-resistant geopolymer produced by granulated blast furnace slag, Miner. Eng. 16 (2003) 205–210.

[22] J. Davidovits, J.L. Sawyer, Early High-strength Mineral Polymer, Patent 4509985, United States, 1985.

[23] J. Davidovits, Method for obtaining a geopolymeric binder allowing to stabilize, solidify and consolidate toxic or waste materials, Patent 5349118, United States, 1994.

[24] S.G. Hu, H.X. Wang, G.Z. Zhang, Q.J. Ding, Bonding and abrasion resistance of geopolymeric repair material made with steel slag, Cem. Concr. Compos. 30 (2008) 239–244.

[25] C.K. Yip, G.C. Lukey, J.S.J. van Deventer, The coexistence of geopolymeric gel and calcium silicate hydrate at the early stage of alkaline activation, Cem. Concr. Res. 35 (2005) 1688–1697.

[26] D. Ravikumar, S. Peethamparan, N. Neithalath, Structure and strength of NaOH activated concretes containing fly ash or GGBFS as the sole binder, Cem. Concr. Compos. 32 (2010) 399–410.

[27] S.D. Wang, K.L. Scrivener, Hydration products of alkali activated slag cement, Cem. Concr. Res. 25 (1995) 561–571.

[28] I.G. Richardson, J.G. Cabrera, The nature of C-S-H in model slag-cements, Cem. Concr. Compos. 22 (2000) 259–266.

[29] S.J. Song, H.M. Jennings, Pore solution chemistry of alkali-activated ground granulated blast-furnace slag, Cem. Concr. Res. 29 (1999) 159–170.

[30] C. Lampris, R. Lupo, C.R. Cheeseman, Geopolymerisation of silt generated from construction and demolition waste washing plants, Waste Manage. 29 (2009) 368–373.

[31] M. Ben Haha, G. Le Saout, F. Winnefeld, B. Lothenbach, Influence of activator type on hydration kinetics, hydrate assemblage and microstructural development of alkali activated blast-furnace slags, Cem. Concr. Res. 41 (2011) 301–310.

[32] J.G.S. Van Jaarsveld, J.S.J. Van Deventer, L. Lorenzen, The potential use of geopolymeric materials to immobilise toxic metals: Part I. Theory and applications, Miner. Eng. 10 (1997) 659–669.

[33] J.I. Escalante-García, A.F. Fuentes, A. Gorokhovsky, P.E. Fraire-Luna, G. Mendoza-Suarez, Hydration products and reactivity of blast-furnace slag activated by various alkalis, J. Am. Ceram. Soc. 86 (2003) 2148–2153.

[34] M. Ben Haha, B. Lothenbach, G. Le Saout, F. Winnefeld, Winnefeld, Influence of slag chemistry on the hydration of alkali-activated blast-furnace slag—Part II: Effect of Al_2O_3, Cem. Concr. Res. 42 (2012) 74–83.

[35] T.D. Ciach, J.E. Gillott, E.G. Swenson, P.J. Sereda, Microstructure of calcium silicate hydrates, Cem. Concr. Res. 1 (1971) 13–25.

[36] A.H. Lav, M.A. Lav, Microstructural development of stabilized fly ash as pavement base material, J. Mater. Civil Eng. 12 (2000) 157–163.

[37] M. Choquette, M.A. Berube, J. Locat, Mineralogical and microtextural changes associated with lime stabilization of marine clays from eastern Canada, Appl. Clay Sci. 2 (1987) 215–232.

[38] M. Chi, Effects of dosage of alkali-activated solution and curing conditions on the properties and durability of alkali-activated slag concrete, Constr. Build. Mater. 35 (2012) 240–245.

[39] T. Bakharev, J.G. Sanjayan, Y.B. Cheng, Effect of elevated temperature curing on properties of alkali-activated slag concrete, Cem. Concr. Res. 29 (1999) 1619–1625.

[40] E. Altan, S.T. Erdoğan, Alkali activation of a slag at ambient and elevated temperatures, Cem. Concr. Compos. 34 (2012) 131–139.

[41] R.B. Kogbara, A. Al-Tabbaa, Mechanical and leaching behaviour of slag-cement and lime-activated slag stabilised/solidified contaminated soil, Sci. Total Environ. 409 (2011) 2325–2335.

[42] B. Kostura, H. Kulveitová, J. Leško, Blast furnace slags as sorbents of phosphate from water solutions, Water Res. 39 (2005) 1795–1802.

[43] S.Y. Oh, S.W. Cha, I.H. Kim, H.W. Lee, S.G. Kang, S.J. Choi, Disposal of heavy metal-contaminated sediment from Ulsan Bay, South Korea: Treatment processes and legal framework, Water Environ. J. 25 (2011) 445–455.

[44] X.G. Li, Y. Lv, B.G. Ma, Q.B. Chen, X.B. Yin, S.W. Jian, Utilization of municipal solid waste incineration bottom ash in blended cement, J. Cleaner Prod. 32 (2012) 96–100.

[45] S. Bouzalakos, A.W.L. Dudeney, C.R. Cheeseman, Controlled low-strength materials containing waste precipitates from mineral processing, Miner. Eng. 21 (2008) 252–263.

[46] S. Diamond, Cement Paste microstructure—An overview at Several Levels, in: Hydraulic Cement Pastes: Their Structure and Properties, Cement and Concrete Association, Sheffield, UK, 1976, pp. 2–30.

[47] R. Alizadeh, J.J. Beaudoin, L. Raki, Mechanical properties of calcium silicate hydrates, Mater. Struct. 44 (2011) 13–28.

[48] I.G. Richardson, G.W. Groves, The incorporation of minor and trace elements into calcium silicate hydrate (C-S-H) gel in hardened cement pastes, Cem. Concr. Res. 23 (1993) 131–138.

[49] I.G. Richardson, The nature of C-S-H in hardened cements, Cem. Concr. Res. 29 (1999) 1131–1147.

[50] D.W. Foreman Jr., Neutron and X-ray diffraction study of $Ca_3Al_2(O_4D_4)_3$, a garnetoid, J. Chem. Phys. 48 (1968) 3037–3041.

[51] G.A. Lager, T. Armbruster, J. Faber, Neutron and X-ray diffraction study of hydrogarnet $Ca_3Al_2(O_4H_4)_3$, Am. Miner. 72 (1987) 756–765.

[52] T. Armbruster, G.A. Lager, Oxygen disorder and the hydrogen position in garnet-hydrogarnet solid solutions, Eur. J. Miner. 1 (1989) 363–369.

[53] B.J. Skinner, Physical properties of end-members of the garnet group, Am. Miner. 41 (1956) 428–436.

[54] J.M. Rivas Mercury, X. Turrillas, A.H. de Aza, P. Pena, Calcium aluminates hydration in presence of amorphous SiO_2 at temperatures below 90℃, J. Solid State Chem. 179 (2006) 2988–2997.

[55] A. Gruskovnjak, B. Lothenbach, L. Holzer, R. Figi, F. Winnefeld, Hydration of alkali-activated slag: Comparison with ordinary Portland cement, Adv. Cem. Res. 18 (2006) 119–128.

[56] F. Puertas, A. Fernández-Jiménez, Mineralogical and microstructural characterisation of alkali-activated fly ash/slag pastes, Cem. Concr. Compos. 25 (2003) 287–292.

[57] B. Lothenbach, A. Gruskovnjak, Hydration of alkali-activated slag: Thermodynamic modelling, Adv. Cement Res. 19 (2007) 81–92.

[58] L. Fernandez, C. Alonso, A. Hidalgo, C. Andrade, The role of magnesium during the hydration of C_3S and C-S-H formation. Scanning electron microscopy and mid-infrared studies, Adv. Cem. Res. 17 (2005) 9–21.

[59] A. Nonat, The structure and stoichiometry of C-S-H, Cem. Concr. Res. 34 (2004) 1521–1528.

[60] J.J. Chen, J.J. Thomas, H.F.W. Taylor, H.M. Jennings, Solubility and structure of calcium silicate hydrate, Cem. Concr. Res. 34 (2004) 1499–1519.

[61] M.J.A. Qomi, K.J. Krakowiak, M. Bauchy, K.L. Stewart, R. Shahsavari, D. Jagannathan, D.B. Brommer, A. Baronnet, M.J. Buehler, S. Yip, F.J. Ulm, K.J. Van Vliet, R.J.M. Pellenq, Combinatorial molecular optimization of cement hydrates, Nat. Commun. 5 (2014) 5960.

[62] M.Y.A. Mollah, M. Kesmez, D.L. Cocke, An X-ray diffraction (XRD) and Fourier transform infrared spectroscopic (FT-IR) investigation of the long-term effect on the solidification/stabilization (S/S) of arsenic(V) in Portland cement type-V, Sci. Total Environ. 325 (2004) 255–262.

[63] T. Richard, L. Mercury, F. Poulet, L. d'Hendecourt, Diffuse reflectance infrared Fourier transform spectroscopy as a tool to characterise water in adsorption/confinement situations, J. Colloid Interface Sci. 304 (2006) 125–136.

[64] T. Uchino, T. Sakka, M. Iwasaki, Interpretation of hydrated states of sodium silicate glasses by infrared and Raman analysis, J. Am. Ceram. Soc. 74 (1991) 306–313.

[65] T. Uchino, T. Sakka, K. Hotta, M. Iwasaki, Attenuated total reflection Fourier-transform infrared-spectra of a hydrated sodium-silicate glass, J. Am. Ceram. Soc. 72 (1989) 2173–2175.

[66] M.Y.A. Mollah, W.H. Yu, R. Schennach, D.L. Cocke, A Fourier transform infrared spectroscopic investigation of the early hydration of Portland cement and the influence of sodium lignosulfonate, Cem. Concr. Res. 30 (2000) 267–273.

[67] T.L. Hughes, C.M. Methven, T.G.J. Jones, S.E. Pelham, P. Fletcher, C. Hall, Determining cement composition by Fourier transform infrared spectroscopy, Adv. Cem. Based Mater. 2 (1995) 91–104.

[68] J.T. Kloprogge, R.D. Schuiling, Z. Ding, L. Hickey, D. Wharton, R.L. Frost, Vibrational spectroscopic study of syngenite formed during the treatment of liquid manure with sulphuric acid, Vib. Spectrosc. 28 (2002) 209–221.

[69] M.A. Trezza, A.E. Lavat, Analysis of the system $3CaO \cdot Al_2O_3$-$CaSO_4 \cdot 2H_2O$-$CaCO_3$-H_2O by FT-IR spectroscopy, Cem. Concr. Res. 31 (2001) 869–872.

[70] P. Yu, R.J. Kirkpatrick, B. Poe, P.F. McMillan, X. Cong, Structure of calcium silicate hydrate (C-S-H): Near-, Mid-, and Far-infrared spectroscopy, J. Am. Ceram. Soc. 82 (1999) 742–748.

[71] M.Y.A. Mollah, F. Lu, D.L. Cocke, An X-ray diffraction (XRD) and Fourier transform infrared spectroscopic (FT-IR) characterization of the speciation of arsenic (V) in Portland cement type-V, Sci. Total Environ. 224 (1998) 57–68.

[72] G.E. De Benedetto, R. Laviano, L. Sabbatini, P.G. Zambonin, Infrared spectroscopy in the mineralogical characterization of ancient pottery, J. Cultural Heritage 3 (2002) 177–186.

[73] A. Fernández-Jiménez, A. Palomo, Mid-infrared spectroscopic studies of alkali-activated fly ash structure, Microporous Mesoporous Mater. 86 (2005) 207–214.

[74] N.J. Clayden, S. Esposito, A. Aronne, P. Pernice, Solid state 27Al NMR and FTIR study of lanthanum aluminosilicate glasses, J. Non-Crystalline Solids 258 (1999) 11–19.